High-Pressure High-Temperature Synthesis of Intermetallic Compounds

Ulrich Schwarz, Lev Akselrud, Michael Baitinger, Ulrich Burkhardt, Wilder Carrillo-Cabrera, William Clark, Julia Hübner, Primoz, Kozelj, Mitja Krnel, Katrin Meier-Kirchner, Teuta Neziraj, Yurii Prots, Sahana Rößler, Walter Schnelle, Katharina Ueltzen, Steffen Wirth and Yuri Grin*

At ambient pressure, the chemical behavior of silicon and germanium in compounds with metals of the alkaline-earth and rare-earth metal groups is characterized by the formation of Zintl phases. Synthesis at high-pressure high-temperature conditions develops the spectrum of existing motifs substantially by granting access to tetrel-rich intermetallic compounds and often surprising bonding properties.

The application of high-pressure high-temperature synthesis techniques paves the way for synthesizing novel atomic arrangements expanding the already impressive diversity of intermetallic compounds. Compression of solid phases in general causes both continuous contractions of interatomic distances and structural phase transitions into denser high-pressure modifications [1]. However, here we focus on high-pressure high-temperature synthesis as a means to achieve previously unrealized compositions establishing new structure motifs and physical properties. Emphasis will be directed to compounds of element semiconductors in group 14, i.e. silicon and germanium.

In the last two decades, high-pressure high-temperature synthesis provided access to a variety of new intermetallic compounds. The already broad spectrum of compositions accessible at ambient conditions has been significantly extended by realizing chemical reactions at extreme reaction conditions yielding numerous new silicon- and germanium-richer compounds (Table 1 and Table 2). Among these, some show superconducting properties like Sr_8Si_{46} [2], MSi_3 (M = Ca, Y, Lu [3]) or MGe_3 (M= Ca, Ba, Lu [4-6]). Application of high-pressure techniques was also successful for synthesizing the new superconductors $CoBi_3$ [7] and CuBi [8] of bismuth.

Tab. 1: Overview of binary high-pressure phases of silicon.

Compound	Metals
MSi_6	M = Ca, Sr, Ba, Eu
$M_{8-x}Si_{46}$	M = C s ($0.2 \leq x \leq 1.1$) M = Sr (x = 0)
MSi_5	M = Mg; Ce, Gd
M_2Si_7	M = Ce
MSi_3	M = Ca; Y, Lu; Yb; Sm, Gd, Tb, Dy, Ho, Er, Tm

Tab. 2: Overview of binary high-pressure phases of germanium.

Compound	Metals
MGe_6	M = Ca, Sr, Ba, Eu
M_8Ge_{46-x}	M = Cs (x = 1.6)
MGe_{6-x}	M = Sr, Ba
MGe_5	M = Ba, Nd, Sm, Gd, Tb
M_2Ge_9	M = Nd, Sm
MGe_3	M = Ca, Ba, Eu; Lu

The formation of unusual polyanionic frameworks by the *p*-block elements Si or Ge in the range of tetrel-rich compositions motivated analysis of the chemical bonding by real-space methods (see **CMS_04_Wagner**). The results evidence that the polyanions are typically characterized by the appearance of multiatomic covalent interactions [9]. Binary phases with exclusively four-bonded framework atoms like MSi_6 or $M_{8-x}Si_{46}$ are characterized by holding excess electrons as indicated by the balance $M^{2+}[(4b)Tt_6^0] \times 2e$. In case of $MgSi_5$ and Sr_8Si_{46}, these induce the formation of previously unknown covalent interactions between host framework and metal guest atoms [2,10]. In compounds like $BaGe_{6-x}$, the formation of defects compensates for the excess in the electron balance as each vacancy gives rise to four negatively charged atoms $(3b)Ge^-$. Thus, the defects effectively act as electron traps, and the vacancies may cause incommensurate modulations of the crystal structure, which require methods of four-dimensional crystallography for refinement and description [11].

A topic of current interest are intermetallic clathrates, tetrel compounds characterized by a covalent host framework of four-bonded atoms harboring metal guests being located in different types of polyhedral

cages. The broad range of diverse chemical compositions opens comprehensive opportunities for shaping their physical properties.

The greater part of clathrates adopts type-I motifs holding 20- and 24-atom cages, another frequent variety is the clathrate-II structure with 20- and 28-atom cages. The crystal structure of the rare type-VIII clathrate offers 20-atom polyhedrons exclusively and is, thus, favorable for hosting guest atoms of small radii (Figure 1). High-pressure techniques are a natural choice for syntheses of clathrate-VIII phases as their atomic arrangement is denser packed than that of the clathrate-I crystal structures. Aiming at new representatives of this infrequent structure pattern, efforts are concentrated on boron-silicon networks.

Conducting synthesis at pressures between 6 and 8 GPa yields a mixture of silicoboride phases [12] from the raw product and thinned by the focused ion beam technique. Structure solution from electron-diffraction data recorded with the precession method reveal a clathrate-VIII-type crystal structure. For the final least-squares refinement of parameters, single-crystal X-ray diffraction data were measured. The parameters indicate a reduced electron density on one of the four atomic positions of silicon, which is interpreted as partial replacement of silicon by boron. The resulting model (Figure 1) with composition $Na_8B_ySi_{46-y}$ ($3 \le y \le 5$) results in realistic interatomic distances and the refined composition is consistent with energy-dispersive X-ray spectroscopy analysis data.

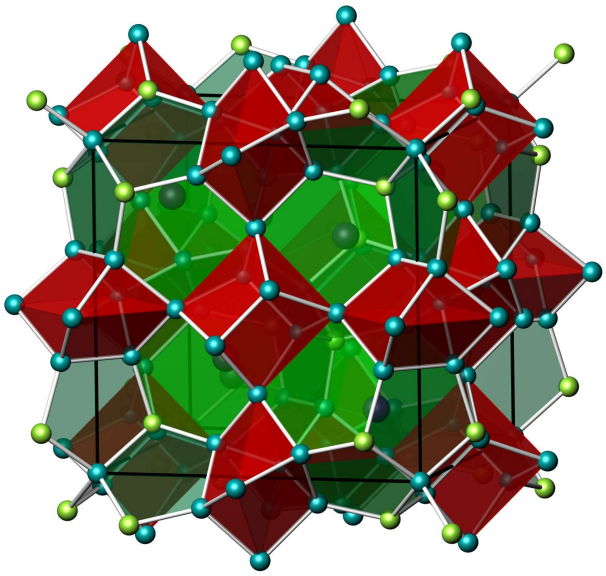

Fig. 1: Crystal structure of the clathrate-VIII $Na_8B_ySi_{46-y}$ ($3 \le y \le 5$).

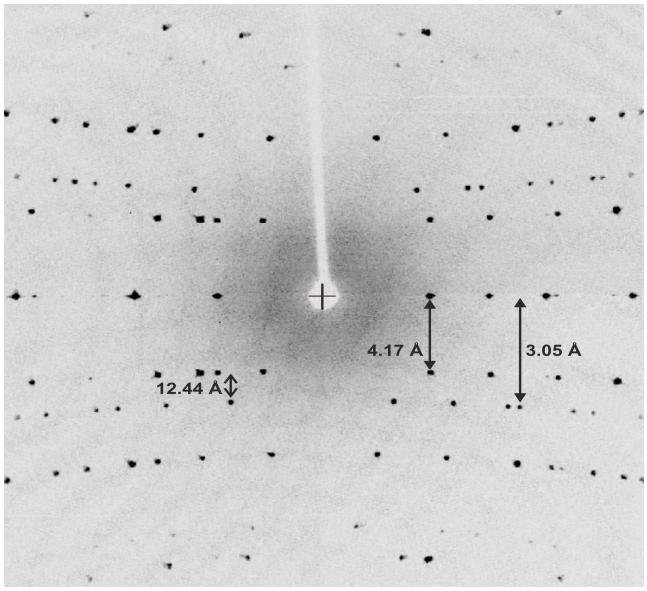

Fig. 2: Rotation photograph of $Mg_9Ge_{5.1(2)}$ around [001]. The diffraction pattern clearly indicates a composite arrangement with two different identity periods of the reciprocal lattice.

Binary compounds of tetrel-elements and alkaline-earth metals form a variety of electron-precise phases at ambient pressure, e.g., the compound Mg_2Ge forms a salt-like fluorite-type crystal structure. High pressure induces the formation of a new phase with a modulated atomic arrangement, which was described as being seemingly related to the pattern of $PbCl_2$ [13]. Our re-investigation by means of single-crystal X-ray diffraction yields a new structure model [14]. The diffraction data can be separated into two subsets, one with identity periods a = 7.2227(8) Å and c = 4.1736(6) Å (Figure 2). The observed second set of reflections is compatible with a modulation vector q^* = 1/3,1/3,~4/3. Alternatively, all reflection positions (Figure 2) may be described by two sublattices with the same orientation and identity periods $a = b \approx \sqrt{3} \times 7.22$ Å and different lattice parameters in direction [001], $c1 \approx 4.17$ Å and $c2 \approx 3.05$ Å.

The absence of systematic extinctions is consistent with space group P3, and the established positions of all magnesium and part of the germanium atoms correspond to the arrangement of UCl_3. This host substructure shows columns of germanium-centered tricapped trigonal prisms Mg_9Ge1, which are connected by sharing the basal planes. The resulting channels contain significant electron density, which are interpreted as a second type of germanium atoms. Combined, the atomic arrangement of $Mg_9Ge_{5.1}$ (Figure 3) may be

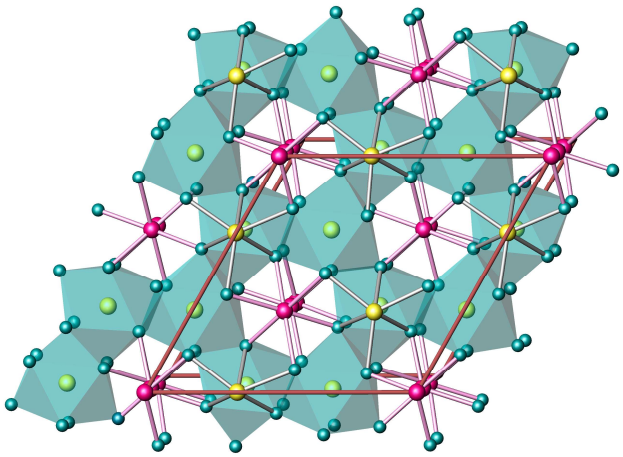

Fig. 3: UCl_3-type framework with ordered magnesium (yellow) and germanium atoms (green) as well as modulated and disordered germanium atoms (pink) in the resulting channels.

described as a UCl_3-type framework of Mg_9Ge1 polyhedrons with modulated and additionally disordered germanium atoms in channels oriented parallel to the *c*-axes.

A large number of investigations has been devoted to high-pressure phases of silicon or germanium with alkaline, alkali-earth or rare-earth metals. In contrast, studies of analogous transition metal compounds are rare. This shortfall motivates the reinvestigation of the cubic body-centered high-pressure phase 'Ge4Co' [15]. Already initial high-pressure high-temperature syntheses point at a different composition of the compound. For addressing the issue, particles of the phase are separated from the product mixture and investigated by scanning electron microscopy. After having prepared an appropriate specimen by the focused-ion-beam lift-out technique, precession electron diffraction tomography data are collected. They confirm cubic body centred symmetry (space group Im-3*m*), but the identified atomic positions indicate a higher cobalt content. Subsequent syntheses with cobalt-richer starting mixtures yield single crystals suitable for X-ray diffraction. Refinement of these data indicate a composition corresponding to $Ge_{32}Co_{9-x}$ ($x = 0.54$) evidencing cobalt deficiency at one position of the TEM structure model [16].

The refined atomic arrangement (Figure 4) contains an approximately primitive cubic grouping of germanium atoms. Such an anion pattern is typical for the CsCl type, which is adopted by various intermetallic compounds. Here, all cubes are filled and even in defect varieties of the γ-brass type, only a small number of cubes are empty. By contrast, the cobalt atoms in

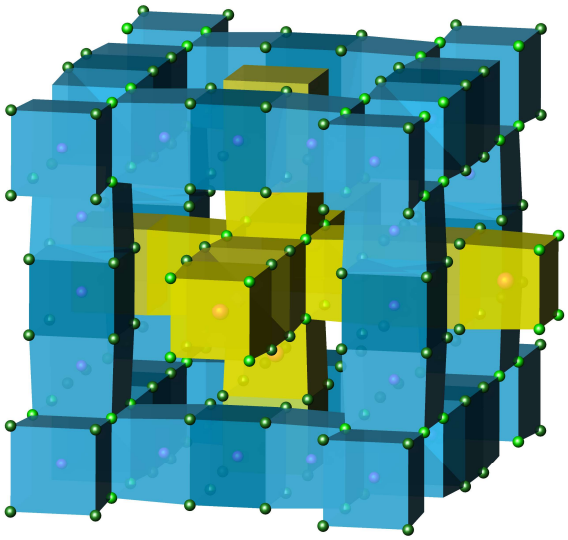

Fig. 4: Crystal structure of $Ge_{32}Co_{9-x}$ with a distorted primitive cubic arrangement of germanium atoms (green). Two frameworks (yellow and blue) of edge- and vertex-connected heteroatomic three-core cluster units interpenetrate.

$Ge_{32}Co_{9-x}$ centre only roughly one quarter of the germanium cubes resulting in empty regions between the frameworks. Such extended voids are often caused by covalent inter-polyhedral bonds or lone pairs. Consequently, the chemical bonding in $Ge_{32}Co_{9-x}$ is investigated by quantum-chemical methods operating in real space.

The topological analysis of the electron density follows the quantum theory of atoms in molecules (QTAIM) [17]. The Co1 species have an effective charge of −0.40, and the Co2 atoms exhibit a charge of −1.20. Accordingly, Ge1 atoms have a charge of +0.48 and Ge2 holds a charge of +1.12. The computed values are positive for germanium and negative for cobalt notifying a transfer which is opposite to that predicted on basis of the usual Pauling scale of electronegativity. However, the finding is in line with the so-called Sanderson plot as well as with recently computed values on basis of the average valence electron energy [15,16].

Topological analysis of the electron-localizability indicator (ELI-D representation) in the diagonal plane of the unit cell shows low values in the center of the empty cubes (Figure 5). Instead, maxima are located close to the edges of these polyhedrons. The analysis identifies seven types of maxima. Of these, conventional two-atomic homopolar bonds Ge2−Ge2 interconnect the two interpenetrating networks resulting in a unique atomic arrangement $Ge_8Ge_{8/3}Co_{3-1/3x}$. Consequently, the bonding is closely associated to the empty

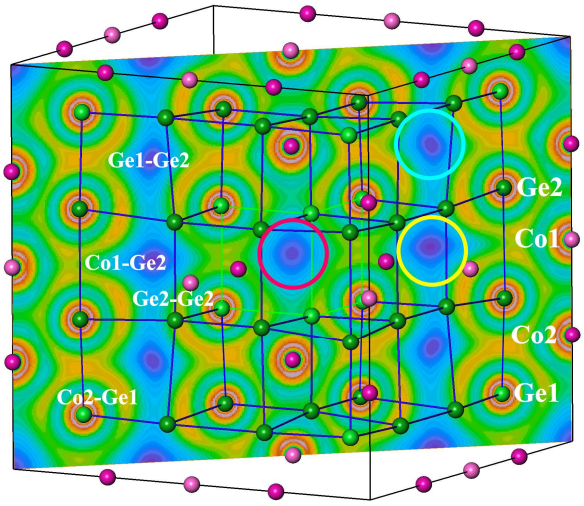

Fig. 5: Electron localizability (ELI-D) distribution in the (10-1) plane of $Ge_{32}Co_{9-x}$. Circles mark the centers of Ge cubes, covalent two-atomic interactions are indicated by white labels of the participating atoms.

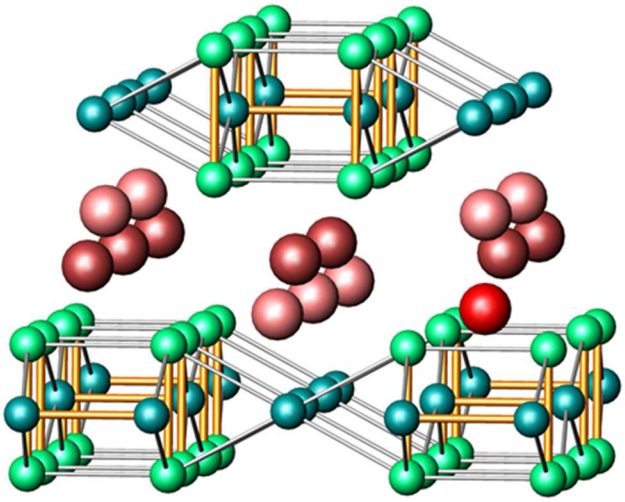

Fig. 6: $YbSi_3$-type crystal structure of $SmSi_3$ with disorder of the samarium atoms (shown in shades of brown). The partially occupied Sm minority position (red) causes defects in the silicon framework (green).

germanium cubes. The one around (000) is stabilized by two-atomic Co2–Ge1 bonds (Figure 5). Also, four edges are formed by two-atomic Ge2–Ge2 bonds between the three-core cluster units, the remaining interactions belong to bonding within the entities. The atoms linked by the Ge2–Ge2 bonds form six-membered Ge rings in chair conformation, which interconnect the frameworks.

Compounds with extended polyanions of tetrel atoms represent an attractive class of materials with respect to structural diversity and physical properties. In a series of reactions at high-pressure, we manufactured a series of phase *RE*Si_3 [17-19] and characterized their magnetic properties [X_COLL_02]. Here, we focus on $SmSi_{3-x}$ (x = 0 - 0.05) featuring extended defects [20]. Metallographic investigation of powder samples $SmSi_3$ disclosed composition $Sm_{25.6(1)}Si_{74.4}$ for the high-pressure phase after synthesis. Refinement of an $YbSi_3$-type crystal structure with powder diffraction data provide no indication for a silicon deficit, but this may be an effect of the large difference in scattering factors between silicon and the heavier rare-earth metal. Structure refinement of single-crystal X-ray diffraction data reveals significant residual electron density of approximately 2.4 $e^-/Å^3$ close to the position of Sm2. This feature is consistent with a third, partially occupied samarium position signaling disorder of the metal atoms. As simultaneous occupation of the positions Sm3 and Sm2 as well as Si2 would result in unreasonable Sm3–Sm2 and Sm3–Si2 distances, the occupation factor of the Sm3 site is coupled to the formation of defects on the sites of Sm2 and Si2. This average model (Figure 6) for $SmSi_{3-x}$ with x = 0.05(2) corresponds to a silicon deficit, which is in qualitative agreement with chemical analysis. The nature of the samarium disorder in the crystal structure is investigated by transmission electron microscopy. In the focused-ion beam cut, dislocations are visible as dark areas in bright-field mode (Figure 7a). The image of a large section clearly shows a dislocation (Figure 7b). A partial displacement of the atomic layers of about 1.1 Å is observed in the selected projection direction, which is consistent with the finding of a partially occupied third samarium position. This is in accord with a nano-domain organization of the regions involving different positions of Sm atoms in the $YbSi_3$-type main matrix.

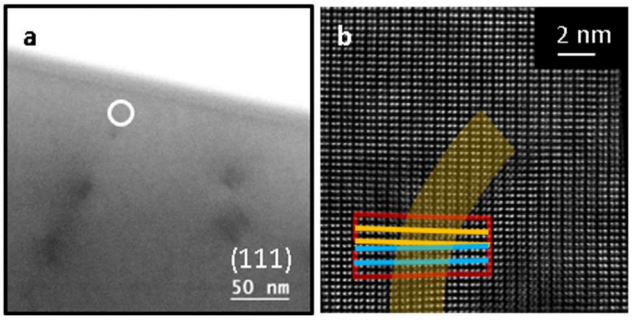

Fig 7: (a) Angular bright-field scanning transmission electron microscopy image of $SmSi_{3-x}$ (b) High-resolution scanning transmission electron microscopy image with dislocations (indicated by the solid red box). Orange and blue lines are guides to the eye.

External Cooperation Partners

Andrew Fitch (ESRF Grenoble, France); Walter Jung (University of Cologne, Germany).

References

[1]* *Crystal Structures and Twinning of $RuBr_3$, Yu. Prots, S. Rößler, U. K. Rößler, H. Rosner, L. Akselrud, M. Schmidt, A. Fitch, U. Schwarz*, Z. Anorg. Allg. Chem.* ***649*** *(2023), e202300140, https://doi.org/10.1002/zaac.202300140*

[2] *In-cage interactions in the clathrate superconductor Sr_8Si_{46}, J.-M. Hübner, Yu. Prots, W. Schnelle, M. Bobnar, M. König, M. Baitinger, P. Simon, W. Carrillo-Cabrera, A. Ormeci, E. Svanidze, Yu. Grin, U. Schwarz, Chem. Eur. J.* ***26*** *(2020) 830-838, https://doi.org/10.1002/chem.201904170*

[3] *Dumbbells of five-connected silicon atoms and superconductivity in the binary silicides MSi_3 (M = Ca, Y, Lu), U. Schwarz, A. Wosylus, H. Rosner, W. Schnelle, A. Ormeci, K. Meier, A. Baranov, M. Nicklas, S. Leipe, C. J. Müller, Yu. Grin, J. Amer. Chem. Soc.* ***134*** *(2012) 13558−13561, https://doi.org/10.1021/ja3055194*

[4] *Dumbbells of five-connected Ge atoms and superconductivity in $CaGe_3$, W. Schnelle, A. Ormeci, A. Wosylus, K. Meier, Yu. Grin, U. Schwarz, Inorg. Chem.* ***51*** *(2012) 5509 -5511, https://doi.org/10.1021/ic300576a*

[5] *Germanium Dumbbells in a New Superconducting Modification of $BaGe_3$, R. Castillo, A. I. Baranov, U. Burkhardt, R. Cardoso-Gil, W. Schnelle, M. Bobnar, U. Schwarz, Inorg. Chem. 5 (2016) 4498-4503 (2016), https://doi.org/10.1021/acs.inorgchem.6b00299*

[6] *Lutetium Trigermanide $LuGe_3$: High-Pressure Synthesis, Superconductivity, and Chemical Bonding, J.-M. Hübner, M. Bobnar, L. Akselrud, Yu. Prots, Yu. Grin, U. Schwarz, Inorg. Chem.* ***57*** *(2018) 10295-10302, https://doi.org/10.1021/acs.inorgchem.8b01510*

[7] *$CoBi_3$: A Binary Cobalt–Bismuth Compound and Superconductor, U. Schwarz, S. Tencé, O. Janson, C. Koz, C. Krellner, U. Burkhardt, H. Rosner, F. Steglich, Yu. Grin, Angew. Chemie Int. Ed.* ***52*** *(2013) 9853-9857, https://doi.org/10.1002/anie.201302397*

[8] *Weak interactions under pressure: hp-CuBi and its analogues, K. Guo, L. Akselrud, M. Bobnar, U. Burkhardt, M. Schmidt, J.-T. Zhao, U. Schwarz, Yu. Grin, Angew. Chemie Int. Ed.* ***56*** *(2017) 5620-5624, https://doi.org/10.1002/anie.201700712*

[9] *Unusual silicon connectivities in the binary compounds $GdSi_5$, $CeSi_5$ and Ce_2Si_7, A. Wosylus, K. Meier, Yu. Prots, W. Schnelle, H. Rosner, U. Schwarz, Yu. Grin, Angew. Chemie Int. Ed.* ***49*** *(2010) 9002-9006, https://doi.org/10.1002/anie.201003490*

[10] *Unconventional Metal-Framework Interaction in $MgSi_5$, J.-M. Hübner, W. Carrillo-Cabrera, Yu. Prots, M. Bobnar, U. Schwarz. Yu. Grin, Angew. Chem. Int. Ed.* ***58*** *(2019) 12914-12918, https://doi.org/10.1002/anie.201907432*

[11] *$BaGe_6$ and $BaGe_{6-x}$: Incommensurately ordered vacancies as electron traps, L. Akselrud, A. Wosylus, R. Castillo, U. Aydemir, Yu. Prots, W. Schnelle, Yu. Grin, U. Schwarz, Inorg. Chem.* ***53*** *(2014)12699-12705, https://doi.org/10.1021/ic5021065*

[12]* *A Borosilicide with Clathrate VIII Structure, J.-M. Hübner, W. Carrillo-Cabrera, P. Kozelj, Yu. Prots, M. Baitinger, U. Schwarz, W. Jung, J. Amer. Chem. Soc.* ***144*** *(2022) 13456-13460, https://doi.org/10.1021/jacs.2c04745*

[13] *Growth of crystals, composite crystal structures and electrical resistance of high-pressure phases of Mg_2B_{1+x} (B=Sn,Ge), N.B. Bolotina, T.I. Dyuzheva, N.A. Bendeliani, V. Petricek, A.F. Petrova, V.I. Simonov, J. Alloys Compd.* ***278*** *(1998) 29-33, https://doi.org/10.1016/S0925-8388(98)00552-0*

[14]* *Order and disorder in the modulated phase hp-$Mg_9Ge_{5.1}$, L. Akselrud, Yu. Prots, J.-M. Hübner, U. Burkhardt, W. Schnelle, Yu. Grin, U. Schwarz, Z. Anorg. Allg. Chem.* ***648*** *(2022) e202100381, https://doi.org/10.1002/zaac.202100381*

[15] *High pressure synthesis and electrical and magnetic properties of $MnGe_4$ and $CoGe_4$, H. Takizawa, T. Sato, M. Shimada, J. Sol. State. Chem.* ***88*** *(1990) 384, https://doi.org/10.1016/0022-4596(90)90232-M*

[16]* *$Ge_{32}Co_{9-x}$: Creating "Empty" Space by High Pressure, W. P. Clark, W. Carrillo-Cabrera, Yu. Prots, A. Fitch, M. Krnel, U. Schwarz, Yu. Grin, Chem. Eur. J.* ***29*** *(2023) e202203955, https://doi.org/10.1002/chem.202203955*

[17] *Atoms in Molecules-A Quantum Theory, R. F. W. Bader, Oxford University Press, New York, 1990.*

[18] *Principles of electronegativity Part I. General nature, R. T. Sanderson, J. Chem. Educ.* ***65*** *(1988) 112-118, https://doi.org/10.1021/ed065p112*

[19] *Electronegativity seen as the ground-state average valence electron binding energy, M. Rahm, T. Zeng, R. Hoffmann, J. Am. Chem. Soc.* ***141*** *(2019) 342-351, https://doi.org/10.1021/jacs.8b10246*

[20]* *Real Structure, Magnetism and Chemical Bonding of $SmSi_{3-x}$, T. Neziraj, Yu. Prots, W. Carrillo-Cabrera, A. Ormeci, S. Wirth, A. Fitch,U. Burkhardt, Yu. Grin, U. Schwarz, Eur. J. Inorg. Chem.* ***27*** *(2023) e202300738, https://doi.org/10.1002/ejic.202300738*

[21]* *Gadolinium trisilicide - a paramagnetic representative of the $YbSi_3$ type series, T. Neziraj, K. Meier-Kirchner, W. Schnelle, S. Wirth, Yu. Grin, U. Schwarz, Z. Naturforsch. B* 77 *(2022) 323-329, https://doi.org/10.1515/znb-2022-0024*

[22]* *Crystal Structure and Magnetic Properties of High-Pressure Phases $RESi_3$ (RE = Tb, Dy, Er, Tm),T. Neziraj, L. Akselrud, S. Wirth, U. Schwarz, Z. Anorg. Allg. Chem.* ***649*** *(2023) e202300119, https://doi.org/10.1002/zaac.202300119*

[#]ulrich.schwarz@cpfs.mpg.de